Tellus (2001), 53A, 526–545
Printed in UK. All rights reserved

TELLUS
ISSN 0280–6495

Linear stability analysis of the three-dimensional thermally-driven ocean circulation: application to interdecadal oscillations

By THIERRY HUCK[1] and GEOFFREY K. VALLIS[2], *Princeton University AOS/GFDL, Princeton, NJ, USA*

(Manuscript received 6 March 2000; in final form 22 March 2001)

ABSTRACT

What can we learn from performing a linear stability analysis of the large-scale ocean circulation? Can we predict from the basic state the occurrence of interdecadal oscillations, such as might be found in a forward integration of the full equations of motion? If so, do the structure and period of the linearly unstable modes resemble those found in a forward integration? We pursue here a preliminary study of these questions for a case in idealized geometry, in which the full nonlinear behavior can also be explored through forward integrations. Specifically, we perform a three-dimensional linear stability analysis of the thermally-driven circulation of the planetary geostrophic equations. We examine the resulting eigenvalues and eigenfunctions, comparing them with the structure of the interdecadal oscillations found in the fully nonlinear model in various parameter regimes. We obtain a steady state by running the time-dependent, nonlinear model to equilibrium using restoring boundary conditions on surface temperature. If the surface heat fluxes are then diagnosed, and these values applied as constant flux boundary conditions, the nonlinear model switches into a state of perpetual, finite amplitude, interdecadal oscillations. We construct a linearized version of the model by empirically evaluating the tangent linear matrix at the steady state, under both restoring and constant-flux boundary conditions. An eigen-analysis shows there are no unstable eigenmodes of the linearized model with restoring conditions. In contrast, under constant flux conditions, we find a single unstable eigenmode that shows a striking resemblance to the fully-developed oscillations in terms of three-dimensional structure, period and growth rate. The mode may be damped through either surface restoring boundary conditions or sufficiently large horizontal tracer diffusion. The success of this simple numerical method in idealized geometry suggests applications in the study of the stability of the ocean circulation in more realistic configurations, and the possibility of predicting potential oceanic modes, even weakly damped, that might be excited by stochastic atmospheric forcing or mesoscale ocean eddies.

1. Introduction

Climate variability occurs on all timescales, from interannual to multimillennial. Although some of the gravest modes, on multimillennial timescales, may be externally forced (for example, by variations in the earth's orbit), many of the interannual ones (like El Niño-Southern Oscillation or the North Atlantic Oscillation) are almost certainly internal modes of variability. As

[1] Corresponding author address: Laboratoire de Physique des Océans, Université de Bretagne Occidentale, UFR Sciences F.308, 6 avenue Le Gorgeu, B.P. 809, 29285 Brest CEDEX, France.
e-mail: thuck@univ-brest.fr
[2] GFDL, Princeton University AOS, Forrestal campus, route 1, Princeton, NJ 08542, USA.
e-mail: gkv@gfdl.noaa.gov

regards decadal-interdecadal timescales, the situation is less clear. Certainly, there appears sustained variability on 60–80 years periods in the Atlantic basin (Kushnir, 1994; Mann et al., 1998; Delworth and Mann, 2000), and variations in the thermohaline circulation are a candidate mechanism to explain such an "Atlantic Multidecadal Oscillation" (Kerr, 2000), although mechanisms external to the ocean–atmosphere system (e.g., variations in atmospheric composition) are also possible. 50–70 years oscillations of the North Atlantic thermohaline cell are found in the Geophysical Fluid Dynamics Laboratory (GFDL) coupled model (Delworth et al., 1993), with sea surface temperatures and salinity patterns comparable to observations. Even assuming a source of variability internal to the ocean–atmosphere system, the mechanism has not been unambiguously identified. On the one hand, it might be a real coupled mode, involving an active role of the atmosphere, as suggested by Timmermann et al. (1998) for the 35-yr oscillation in the Max Planck Institute coupled model; on the other hand it might be a damped thermohaline oscillator excited by stochastic atmospheric forcing (Mikolajewicz and Maier-Reimer, 1990; Delworth and Greatbatch, 2000), with ocean dynamics setting the period. The latter mechanism is robust, but not universal. For example, large-scale ocean models in idealized geometry tend to produce interdecadal oscillations under certain boundary conditions, like fixed surface fluxes of heat and freshwater (Greatbatch and Zhang, 1995) or when coupled to atmospheric energy balance models (Chen and Ghil, 1996), but the oscillations are often damped by topography or by strongly relaxing upper boundary conditions (Huck et al., 2001).

It is important to make a distinction between ocean models' oscillations arising under mixed boundary conditions [that is, relaxation of surface temperature but prescribed freshwater flux, see for example Weaver and Sarachik (1991) and Weaver et al. (1991)], and purely thermally-driven oscillations under fixed heat flux with no salinity. In the former, the oscillation typically emerges when flux boundary conditions on surface salinity (e.g., fixed freshwater fluxes) are used. In the latter case, oscillations arise solely with prescribed sensible heat fluxes, and an additional freshwater flux appears if anything to play a damping role on the variability (Greatbatch and Zhang, 1995), but the mechanisms are sufficiently unclear that a more precise statement is not possible. In the following, we focus for simplicity on the oscillations involving a single density variable, temperature, and the conclusions we draw may not be appropriate for the oscillations under mixed boundary conditions, or for the real ocean.

Considerable effort has gone into exploring the parameter space and forcing regimes associated with the oscillations in such thermally-driven ocean models, trying to determine, among other things, the sensitivity of the oscillations to certain parameters and parameterizations that may be poorly known or ill-understood. For example, it appears that the oscillation's amplitude and period is rather sensitive to the surface forcing — models forced with constant (in time) surface buoyancy flux are much more likely to produce oscillations than models forced by "relaxation" surface conditions, in which the heat flux is typically specified as proportional to the difference between the SST and a specified atmospheric temperature. (Of course relaxing to a specified atmospheric temperature is not particularly realistic on such long time scales (Seager et al., 1995 and others), since the ocean heat capacity largely dominates that of the atmosphere.) The sensitivity to the presence of an active mesoscale has also been explored by way of eddy-permitting simulations (Fanning and Weaver, 1998; Huck et al., 2001). Whereas the variability does lose its regularity, interdecadal periods are clearly sustained with large amplitude, suggesting that energetic mesoscale eddies do not damp the long-term variability, but might rather trigger or excite it, acting as a quasi-stochastic forcing. Overall, it appears that ocean-only models with sufficiently weak dissipation of surface density anomalies, either through atmospheric coupling or some other mechanism, seem able to produce oscillations.

Several theories have been proposed to explain these oscillations, some of them building on the simple Malkus (1972) loop (Greatbatch and Zhang, 1995; Huang and Chou, 1994). Although something of an oversimplification, the lag between the overturning circulation amplitude and changes in the meridional density contrast emerged as a robust causal mechanism in a number of subsequent studies with more complete models (Greatbatch and Peterson, 1996; Huck et al., 1999). Consistently, zonally-averaged

models in which the overturning circulation is diagnostic of the density field, and thus in phase with the meridional density gradient, usually do not reproduce the same kind of oscillatory behavior when only one density variable is used (Winton, 1996; Drbohlav and Jin, 1998; Colin de Verdière and Huck, 2000). The situation appears more complex in case in which both temperature and salinity are allowed to evolve independently, although in such simulations there is a phase differences between meridional overturning, temperature and salinity which may have a similar role. However, this is beyond the scope of this paper.

While the basic oscillator mechanism, at least in a variety of thermally-driven models, seems robust and uncontroversial, the details by which the oscillations are sustained against dissipation is less so. Suggested important processes include viscous boundary waves (analogous to Kelvin waves when time-derivatives are not retained in the momentum equations; Greatbatch and Peterson, 1996) and baroclinic instability (Colin de Verdière and Huck, 1999). In the latter mechanism a form of baroclinic planetary waves realizes the adjustment of the circulation to density changes. The waves feed on the mean potential energy field and maintain their amplitude against the large model dissipation such that oscillations can repeat themselves perpetually. In the truly thermohaline oscillations under mixed boundary conditions both temperature and salinity participate actively as separate dynamical variables and the mechanisms are correspondingly more complex, although the ultimate energy source in both cases is provided through the boundary condition on surface temperature, which in turn maintains the available potential energy of the mean oceanic state.

It is often the case that the thermal oscillations are quite regular (Huck et al., 2000). It is therefore reasonable to ask whether the structure of the oscillations might be represented by a simpler, linear, model. A reasonable first step then is to perform a linear stability analysis, to see if the structure of any resulting instability resembles that in the nonlinear, time-dependent, integrations. This kind of analysis was performed in the early days of baroclinic instability theory with regard to the theory of weather systems, and in some ways the problem here is analogous. We do not necessarily expect that, in reality, very long-term oscillations of the ocean can be represented as an unstable linear mode; at the very least, the mode must equilibrate and this implies some nonlinearity. (If the oscillatory mode is a stable oscillator excited by atmospheric stochastic forcing, damping effects alone are sufficient for equilibration — but this is not the case for the thermally-driven mode forced by perfectly constant surface heat flux.) Nevertheless, a linear instability may be a useful indicator as to whether sustained oscillations are to be expected, and, if the ocean is in fact near a bifurcation point (Tziperman et al., 1994; Tziperman, 1997), it may give some quantitative information about the oscillation. The problem is technically more difficult than that of baroclinic instability in a zonal flow since the basic state is inherently three-dimensional. There is no easy analytic way to specify this state, and thus no analytic way to construct the associated linear model.

In studies of the large-scale ocean circulation, linear stability analysis has thus far been used in mainly two-dimensional flows, both in the meridional plane for studying the multiple steady state of the thermohaline circulation under mixed boundary conditions, and in the horizontal plane with shallow water or quasigeostrophic equations for understanding vacillations of the wind-driven circulation. For example, Schmidt and Mysak (1996) investigated century-scale variability of the thermohaline circulation in zonally averaged ocean models by performing a linear stability analysis of several steady states in an extended parameter regime. Vellinga (1996) obtained bifurcation diagrams of the Navier-Stokes equations and the Wright and Stocker (1992) model for the two-dimensional thermohaline circulation as a function of the amplitude of the surface salinity flux, through a numerical continuation technique and linear stability analysis. In the horizontal plane, numerous studies have looked into the stability and variability of wind-driven single and double gyres for various dynamics in idealized geometry basins and forcing, and these have been shown relevant for more realistic cases (Dijkstra and Molemaker, 1999). For instance Sheremet et al. (1997, and references therein) analyze the stability of a barotropic model of the wind-driven circulation and discuss the structure of the unstable eigenmodes and their dependency

with model parameters and lateral boundary conditions. More recently, Meacham (2000) addresses the bifurcation structure associated with such variability.

In this paper we apply some of these methods to the three-dimensional thermohaline circulation. First, we must obtain a time-independent state from which to perform the analysis. Interesting steady states — that is where a slight change in model parameters or forcing might lead to oscillations — are available to us in two cases. First when the model is run to equilibrium by way of strong relaxation of the surface density: this solution evolves into oscillations when the surface fluxes are diagnosed at the end of the restoring run and the integration continued with the fluxes fixed. Second, when the model solutions are analyzed around a bifurcation point by varying a critical damping parameter (the horizontal tracer diffusion for instance): a slightly supercritical coefficient leads to sustained oscillations while a subcritical coefficient leads to weakly damped oscillations converging to a steady state, whose stability can be analyzed. Given a steady state, we obtain its stability properties by methods to be described below.

In Section 2, we describe the planetary geostrophic model, the numerical method we use to estimate the tangent linear model, the model configuration and the parameters used. In Section 3, we analyze the divergence of a steady state upon a switch from restoring to fixed flux in the surface boundary conditions, and compare the associated eigenmodes with the nonlinear oscillation. In Section 4, we empirically construct a crude bifurcation diagram, by tracking the unstable mode towards the bifurcation, as a function of the horizontal tracer diffusion, which suggests that the instability follows a supercritical Hopf bifurcation. Discussion and conclusions follow in Sections 5 and 6.

2. The planetary geostrophic model and its tangent linear model

Planetary geostrophic models are an efficient and conceptually simple tool for studying the large-scale circulation (Samelson and Vallis, 1997a). Valid for spatial scales much larger than the deformation radius, and for advective time scales, they differ from the hydrostatic primitive equations in their neglect of the time-derivative and nonlinear advective terms in the momentum equations, resulting in diagnostic equations for the velocity fields. Then the linearization of the model equations is somewhat simpler than for the primitive equations since one does not have to keep track of the velocity field. For the large-scale circulation, such simplified models also give solutions that are quite similar to those of primitive equation models, both steady and oscillatory (Greatbatch and Zhang, 1995; Huck et al., 1999). We recall here the model equations and describe the procedure used for computing the tangent linear model.

2.1. *The planetary geostrophic model*

In order to provide a well-posed problem in a closed domain, appropriate frictional or diffusive terms must be included in the momentum or thermodynamic equations (Samelson and Vallis, 1997b). Here we choose a conventional Laplacian form in the horizontal momentum equations, and the equations of motion become:

$$f\boldsymbol{k}\times\boldsymbol{u} = -\frac{1}{\rho_0}\nabla p + v\nabla^2\boldsymbol{u}, \tag{1}$$

$$p_z = \rho_0 \alpha g T, \tag{2}$$

$$\nabla\cdot\boldsymbol{u} + w_z = 0, \tag{3}$$

$$T_t + \nabla\cdot(\boldsymbol{u}T) + (wT)_z = \nabla\cdot(K_H\nabla T) + (K_V T_z)_z, \tag{4}$$

where p is the pressure, $\boldsymbol{u}(w)$ the horizontal (vertical) component of the velocity, z the vertical axis coordinate increasing upward in the direction of $\boldsymbol{k}$, and the operator ∇ is restricted to the horizontal coordinates. The equations are solved on a Cartesian β-plane such that the Coriolis parameter is given by $f = f_0 + \beta(y - y_0)$. The Boussinesq approximation is used with the density ρ being linearly related to the temperature T by $\rho = \rho_0[1 - \alpha(T - T_0)]$, where ρ_0 is a reference value ($1023\ \mathrm{kg\ m^{-3}}$) and α the thermal expansion coefficient ($2\times10^{-4}\ \mathrm{K^{-1}}$). Finally v and K_H are the horizontal eddy viscosity and diffusivity coefficients, both uniform.

As stated in the introduction, we do not include salinity and in so doing sacrifice realism for simplicity. Similarly, in the experiments we describe in most detail the wind forcing is set to zero, although

we introduce it later in experiments that partially explore the parameter space. Accordingly bottom friction is set to zero. No-slip boundary conditions are imposed on the lateral boundaries. The circulation is simply driven through a differential heat flux Q occurring through the ocean surface where $K_V T_z = Q/(\rho_0 C_P)$, with C_P the specific heat capacity of seawater (4000 J kg^{-1} K^{-1}).

The linearization of convection schemes is a recurrent concern for the estimation of tangent linear and adjoint models, as used for both atmospheric and oceanographic assimilation purposes (for instance, Tziperman et al., 1992; Miller et al., 1994; Zou, 1997). Rather than a full convective adjustment (which is a nonlocal process in a nonlinear model, and thus not representable by partial differential equations and difficult to linearize) convection is parameterized here through a spatially and temporally varying vertical mixing coefficient K_V depending on the vertical density gradient: When the stratification is stable between two superposed gridboxes, K_V takes the background vertical diffusion value K_0 at the interface, whereas for unstable stratification, K_V takes a very large convective diffusion value K_C equal to 10 m^2 s^{-1}, following the non-hydrostatic three-dimensional numerical experiments of Klinger et al. (1996). Comparisons with the full convection scheme show differences lower than 10^{-4}°C in transients and steady states. The scheme using an enhanced diffusivity is, although more local than the full scheme, unfortunately still locally non-differentiable because of the step function of the vertical density gradient. However, we are now able to (numerically) obtain an associated tangent linear model, as will be described. We do not use here a fully differentiable convection scheme (as discussed towards the end of the next section) because of the sensitivity of the model oscillations to even slightly unresolved static instabilities that may then occur.

2.2. *The tangent linear model*

The finite difference discretization of the planetary geostrophic equations can be written symbolically as the nonlinear system:

$$\dot{T}_i = \mathscr{F}_i(\{T_i\}) = \mathrm{F}_{ij} T_j,$$

where the nonlinear function $\mathscr{F}$ depends on the various elements T_i of the temperature field T on the three-dimensional grid. This can always be written formally as a matrix F whose elements (F_{ij}) are nonlinear (and nontrivial) functions of (T_i), the model parameters and the forcing, multiplying the temperature field.

Given a perturbation (δT_i) around a state (T_i), the linearized evolution of the perturbation is formally given by:

$$\begin{aligned} T_i + \delta T_i &= F_{ij}|_{(T_i+\delta T_i)}(T_j + \delta T_j) \\ &= F_{ij}|_{(T_i)} T_j + \left[F_{ij}|_{(T_i)} + \left.\frac{\partial F_{ij}}{\partial T_k}\right|_{(T_i)} T_k \right] \delta T_j \\ &\quad + \mathrm{O}(|\delta T_j^2|). \end{aligned} \tag{5}$$

If (T_i) is a steady-state $(F_{ij} T_j \equiv 0)$, the linearization simplifies as

$$\begin{aligned} \delta \dot{T}_i &= A_{ij} \delta T_j \\ &= \left[F_{ij}|_{(T_i)} + \left.\frac{\partial F_{ij}}{\partial T_k}\right|_{(T_i)} T_k \right] \delta T_j + \mathrm{O}(|\delta T_j^2|), \end{aligned} \tag{6}$$

where A is the tangent linear matrix at (T_i), also known as the Jacobian of $\mathscr{F}$. The adjoint operator, commonly used for sensitivity studies and data assimilation, is simply the transpose of A.

Due to the overall complexity of the model (especially the locally non-differentiable nature of the convection scheme and the non-local solution of the elliptic equation solved each time step for determining the horizontal velocities) the elements of the tangent linear matrix coefficients (A_{ij}) are evaluated in a purely numerical manner. Once a steady state is reached (say under restoring surface boundary conditions or with large horizontal tracer diffusivity), each grid-point value of the solution T_j is successively perturbed by a small amount δT_j (typically about 0.05°C) and the full model is run forward for several time steps but for period Δt very short compared to the typical time scale of the system, $\mathrm{O}(\Delta x/U)$. Typically we run the model for a week, with time steps of 1 day. Given a small positive perturbation at gridpoint j the steady state T_i evolves into a new slightly perturbed state (call it T_i^{j+}). We repeat the nonlinear integration for a perturbation of opposite sign $-\delta T_j$, which leads to the new perturbed state (T_i^{j-}). The tangent linear matrix coefficients for column j are then estimated as the induced deviation of each gridpoint temperature $\Delta T_i^j = T_i^{j+} - T_i^{j-}$ divided by the integration length Δt

and the total perturbation $2\delta T_j$:

$$A_{ij} = \frac{\delta \dot{T}_i}{\delta T_j} \simeq \frac{\Delta T_i^j}{2\Delta t\, \delta T_j} \simeq \frac{T_i^{j+} - T_i^{j-}}{2\Delta t\, \delta T_j}. \quad (7)$$

Thus we construct a simple, centered-difference approximation to the tangent linear matrix coefficients. We might also say that we have empirically computed the impulse-response matrix of the system. Stammer and Wunsch (1996) have used a comparable semi-automatic linearization of a primitive-equation ocean general circulation model for computing model Green functions for use in altimetry assimilation.

The centered form of the derivative approximation (versus a single-sided derivative for instance) is crucial because of the different behavior of convection regarding positive and negative temperature anomalies. The resulting tangent linear matrix estimate (and its eigenvalues and eigenmodes) appears to be rather insensitive to the amplitude of the temperature perturbation (within the tested range 0.01–0.5°C) and to the model integration duration (within the range 1–15 days), as well as to the accuracy of the steady state (whether the model is run 1000 or 3000 years under restoring boundary conditions), at least for the dozen most unstable eigenmodes that we will compute and analyze in the following.

Our procedure of calculating the tangent linear model suffices for our purposes, but it is not the most general procedure available. For example, various techniques are becoming available or are being developed to automatically construct the tangent linear model or the adjoint (Giering, 1999). Schmidt and Mysak (1996) derived analytically the linear tangent model by hand for the simpler two-dimensional thermohaline circulation model of Wright and Stocker (1991, 1992), in which they implemented a fully differentiable convection scheme. Vellinga (1996) also implemented a differentiable convection scheme, and used a pseudo-arclength numerical continuation technique to follow branches of solution and a combination of complex mapping and the Simultaneous Iteration Technique to find the dominant eigenvalues for the linear stability problem (Dijkstra et al., 1995).

Given the matrix A_{ij} we finally compute its eigenmodes using an Arnoldi iterative algorithm to extract a selected number of eigenvalues, typically 20, ordered according to their largest real part. Associated eigenvectors are then computed. The convergence of the algorithm has been checked on smaller and larger matrices (from various model resolutions), and against different methods of eigenanalysis. The sensitivity of the leading eigenvalues and eigenmodes to the discrete derivation method used for estimating the tangent linear matrix in the range of time integration and temperature perturbation indicated in the text is less than 1%.

2.3. *The model configuration*

Because of (initial) numerical limitations in performing the eigenanalysis of the three-dimensional matrix, we use a domain reduced somewhat in vertical size and resolution from that achievable for a forward integration. We use a domain of depth 2850 m with 12 vertical levels of thickness 50×3, 100, 150, 200, 250, 300, 350, 400, 450, 500 m respectively. The horizontal domain is that of a β-plane centered at 40°N, extending from 20°N to 60°N (4480 km) and 5120 km wide (roughly 60° at 40°N, that is almost 45° at the equator), with 24×21 grid points, giving an isotropic grid spacing close to 213 km.

Model parameters are adapted to this coarse-resolution grid, with horizontal viscosity (diffusivity) of 1.5×10^5 (700) $m^2\, s^{-1}$. The vertical diffusivity ($10^{-4}\, m^2\, s^{-1}$) is larger than current realistic estimates to ensure a reasonable meridional overturning of 10 Sv (1 Sverdrup = $10^6\, m^3\, s^{-1}$) within such a limited ocean domain.

The mean circulation features an anticyclonic gyre in the upper layers (thermocline) and a cyclonic gyre at depth, linked through deep water formation along the northern boundary and north-east corner, and upwelling along the southern and western boundary and across the tropical thermocline. It is very similar to that described in earlier papers (Huck et al., 1999).

3. Divergence of a steady state upon a switch of surface boundary condition

We first run the model to a steady state under restoring surface boundary conditions. We then diagnose the implied surface flux field and continue the integration with this fixed. Oscillations develop, and the initially steady solution evolves

into one of steady periodic oscillations. Under such constant flux, the model shows the coexistence of an unstable equilibrium and a stable limit cycle, which, as we will see, is verified through a linear stability analysis of the steady state.

3.1. *The forward integration*

For the restoring boundary condition we use $Q = \gamma(T^* - \mathrm{SST})$ where $T^*(y)$ is given, and with a coupling coefficient $\gamma = 35\ \mathrm{W\ m^{-2}\ K^{-1}}$ (Haney, 1971): this is equivalent to a restoring time scale $\tau = \rho_0 C_P h_m/\gamma = 66$ days for a mixed layer depth h_m equal to the first model level thickness of 50 m. T^* is an equivalent atmospheric temperature chosen as a linear function of latitude only, varying from 25°C at 20°N to 2°C at 60°N. The initial ocean temperature is set uniformly to 4°C. After 1000 years the model is in a steady state, and the surface heat flux field is diagnosed (Fig. 1). The model integration is then continued with the flux held constant: The previous model solution becomes unstable, and 350 years after the shift in surface boundary conditions, the steady state diverges into an oscillatory solution of period 22.5 years (Fig. 2). The time taken for the instability to manifest itself is a function of how close the model is to a precise steady state, and is not useful as a representation of the instability. For example, if the model is integrated longer under restoring boundary conditions, say 1000, 2000 or 3000 years, the solution diverges respectively 350, 650 and 900 years after the shift to fixed flux. The instability develops immediately if small random perturbations are added to the steady state. A typical time scale for the exponential growth can be estimated from the years 1200 to 1600 (Fig. 2b), where the logarithm of the amplitude of the oscillations in terms of total kinetic energy grows linearly with time with a slope of $(58.4\ \mathrm{years})^{-1}$. The oscillations are perfectly regular and almost sinusoidal, but the mean circulation and stratification is slightly shifted from the steady state, with some cooler deep water being formed.

3.2. *Linear stability analysis*

A linear stability analysis of the steady state is performed under both restoring and constant flux boundary conditions. The eigenvalues of the tangent linear model (a 6048^2 matrix) are obtained numerically, using standard libraries. The eigenvalues with the largest real part (i.e., the unstable ones) are given in Table 1, while the vertical structure of some eigenvectors is shown in Fig. 3. In the restoring case, all eigenvalues have negative real part (damped modes) in agreement with the forward model integration leading to a steady state. Several eigenvalues have a rather small negative real part, hence represent weakly damped modes on time scales of several decades, that could certainly be excited through random noise in the surface forcing (synoptic atmospheric disturbances for instance).

In the constant flux case, a single conjugate pair

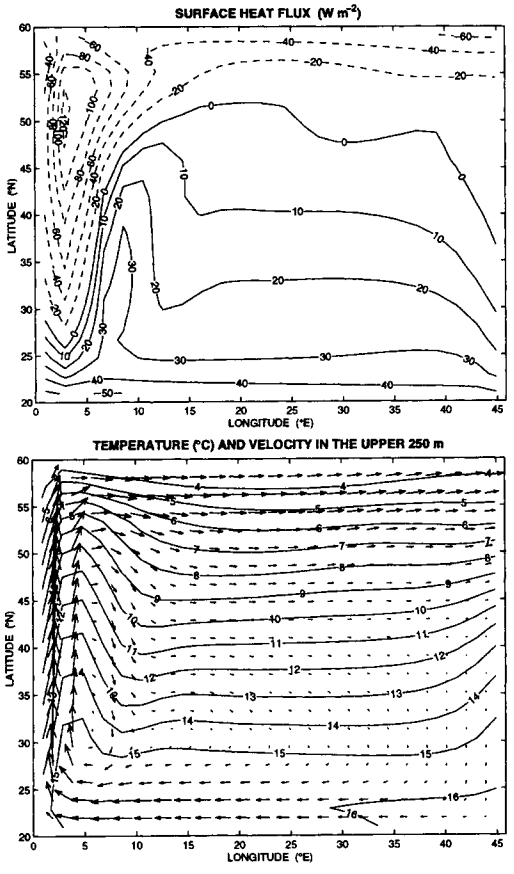

Fig. 1. (a) Surface heat flux ($\mathrm{W\ m^{-2}}$) diagnosed at year 1000 of the model simulation under restoring boundary conditions with a constant $\gamma = 35\ \mathrm{W\ m^{-2}\ K^{-1}}$ to a linear profile of temperature, zonally uniform and linearly varying with latitude from 25°C at 20°N to 2°C at 60°N. (b) Upper 250 m temperature (°C) and velocities (0.5 cm/s per degree).

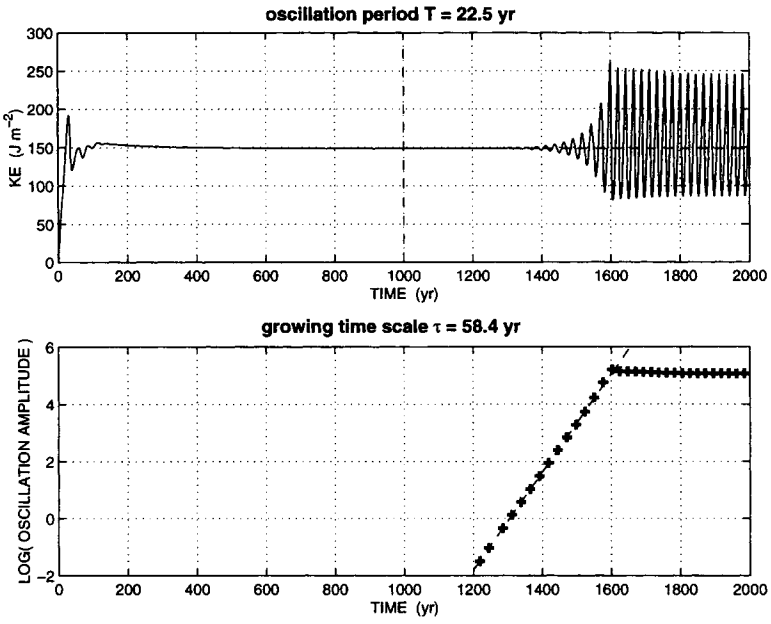

Fig. 2. (a) Time evolution of kinetic energy under restoring boundary conditions (solid line before year 1000, dashed line afterwards) and under fixed heat flux diagnosed at year 1000 (solid line after year 1000). (b) Amplitude of the oscillations (log) as a function of time, the amplitude being measured as the difference between two consecutive extrema.

Table 1. *Eigenvalues of the tangent linear matrix under restoring and fixed flux boundary conditions for the steady state achieved under restoring boundary conditions*

	Restoring: steady state				Diagnosed flux: $T = 22.5$ years, $\tau = 58.4$ years			
	ω_r (yr^{-1})	ω_i (yr^{-1})	τ (yr)	T (yr)	ω_r (yr^{-1})	ω_i (yr^{-1})	τ (yr)	T (yr)
1	−0.0065		−153.8		0.0211	∓0.2485i	47.4	25.3
2	−0.0339		−29.5		−1.35e−5		−7.4e4	
3	−0.0450	∓0.0456i	−22.3	137.8	−0.0147		−67.9	
4	−0.0549		−18.2		−0.0397	∓0.4307i	−25.2	14.6
5	−0.0597	∓0.2762i	−16.8	22.7	−0.0424		−23.6	
6	−0.0792		−12.6		−0.0449	∓0.0392i	−22.3	160.3
7	−0.0866	∓0.0364i	−11.5	172.6	−0.0723		−13.8	

We define the growth (or damping if negative) time scale as $\tau = 1/\omega_r$ and the oscillation period $T = 2\pi/\omega_i$. Note the similarity in imaginary part (as well as in the associated eigenmode spatial structure) of the unstable eigenvalue #1 in the constant flux case with the damped eigenvalue #5 in the restoring case.

of eigenvalues is found with a positive real part, with a growth time scale $\tau = 1/\omega_r = 47.4$ years, while the imaginary period $T = 2\pi/\omega = 25.3$ years. These are to be compared to the timescales of the fully-developed oscillations in the constant flux case, which have growth time-scale of 58.4 years and a period of 22.5 years (Fig. 2). In several other experiments with various resolution and geometry configuration, the model fully-developed oscillations periods (ranging from 16 to 42 years) compared well, i.e., within a few years, to the unstable mode imaginary period.

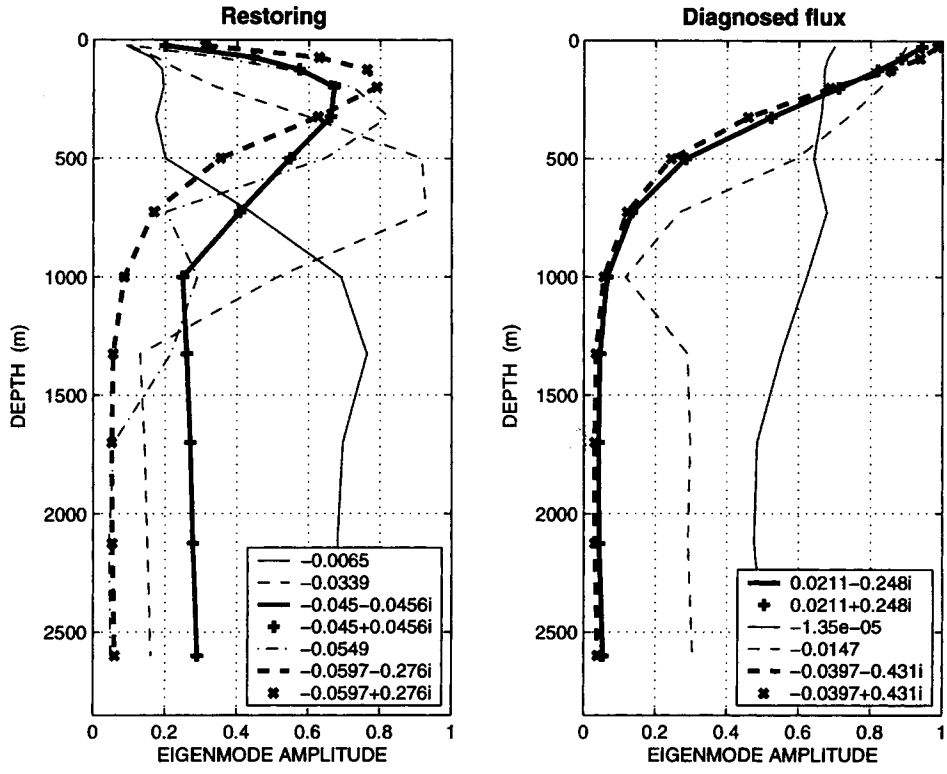

Fig. 3. Vertical structure of some eigenmodes for the model under (a) restoring boundary conditions and (b) fixed heat flux diagnosed after the restoring run. The eigenmode amplitude is defined as the horizontal average of the absolute value or complex modulus of the eigenvector. Note the intense surface damping of all the modes under restoring boundary conditions.

The spatial structure of the linearly unstable mode reveals a large scale pattern intensified in the north-west quarter of the domain: Both real and imaginary part have their main structure (of opposite signs) centered close to 50°N, 5–15°E, especially in the upper layers. There is a significant shift of the horizontal pattern with depth (Fig. 4). Since the model solution is limited to the real plane, the complex conjugate eigenvalues $(\omega_r \pm i\omega_i)$ are associated with complex conjugate eigenvectors $(V_r \mp V_i)$. Letting aside the growth rate, which only modulates the amplitude of the oscillation, the time evolution due to the imaginary part of the eigenvalue follows: $V(t) = \cos(\omega_i t)V_r + \sin(\omega_i t)V_i$. The evolution of sea surface temperature anomaly shows a relatively stationary pattern in the north-west corner, alternatively positive and negative, the phase shift being initiated by advection of anomalies through changes in the western boundary current transport (Fig. 5, left column). At deeper levels (700–1700 m), the temperature anomalies seem to originate from the north-east corner and propagate westward along the northern boundary, then southward along the western boundary and vanish.

The structure of the unstable mode under diagnosed heat flux (eigenvalue #1) closely resembles a decaying (i.e., negative real part of the eigenvalue) oscillatory eigenmode obtained under restoring boundary conditions (eigenvalue #5, not shown). Except for the relative amplitude of the surface anomalies compared to deeper levels, the horizontal patterns are very similar in the upper levels and associated with the western boundary current and its eastward extension. At greater depths (700–1700 m), the westward propagating wave-like structure along the northern boundary

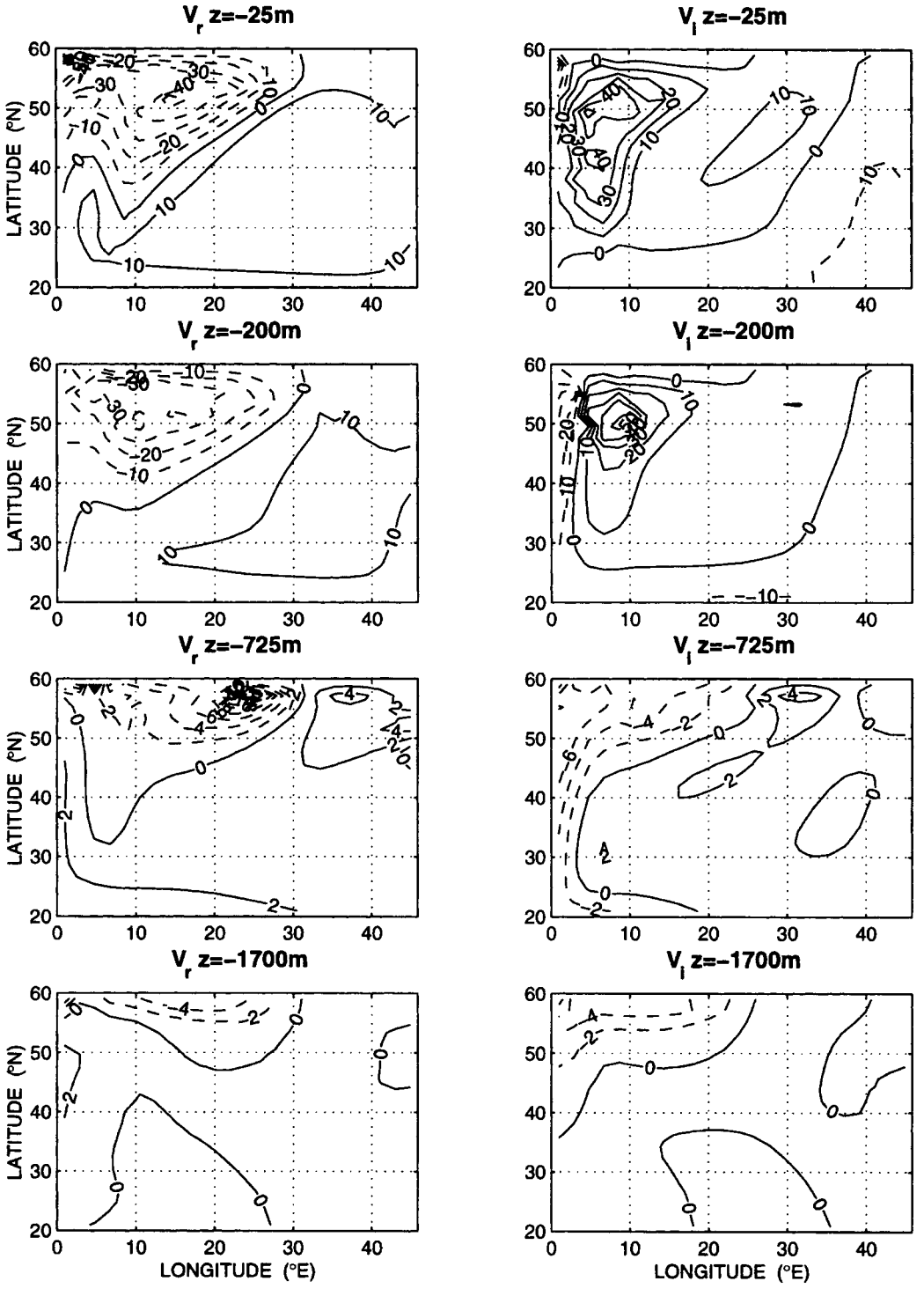

Fig. 4. Horizontal structure at various depths of the only unstable eigenmode of temperature for the tangent linear matrix of the model under constant surface heat flux diagnosed after a restoring run: The real and imaginary part of the eigenvector associated with the only pair of conjugate eigenvalues (#1) with positive real part correspond to phases of an oscillation of growing amplitude a quarter period apart or 6.3 years here ($V_r \rightarrow V_i \rightarrow -V_r \rightarrow -V_i \rightarrow V_r \ldots$). Note that the amplitude is arbitrary.

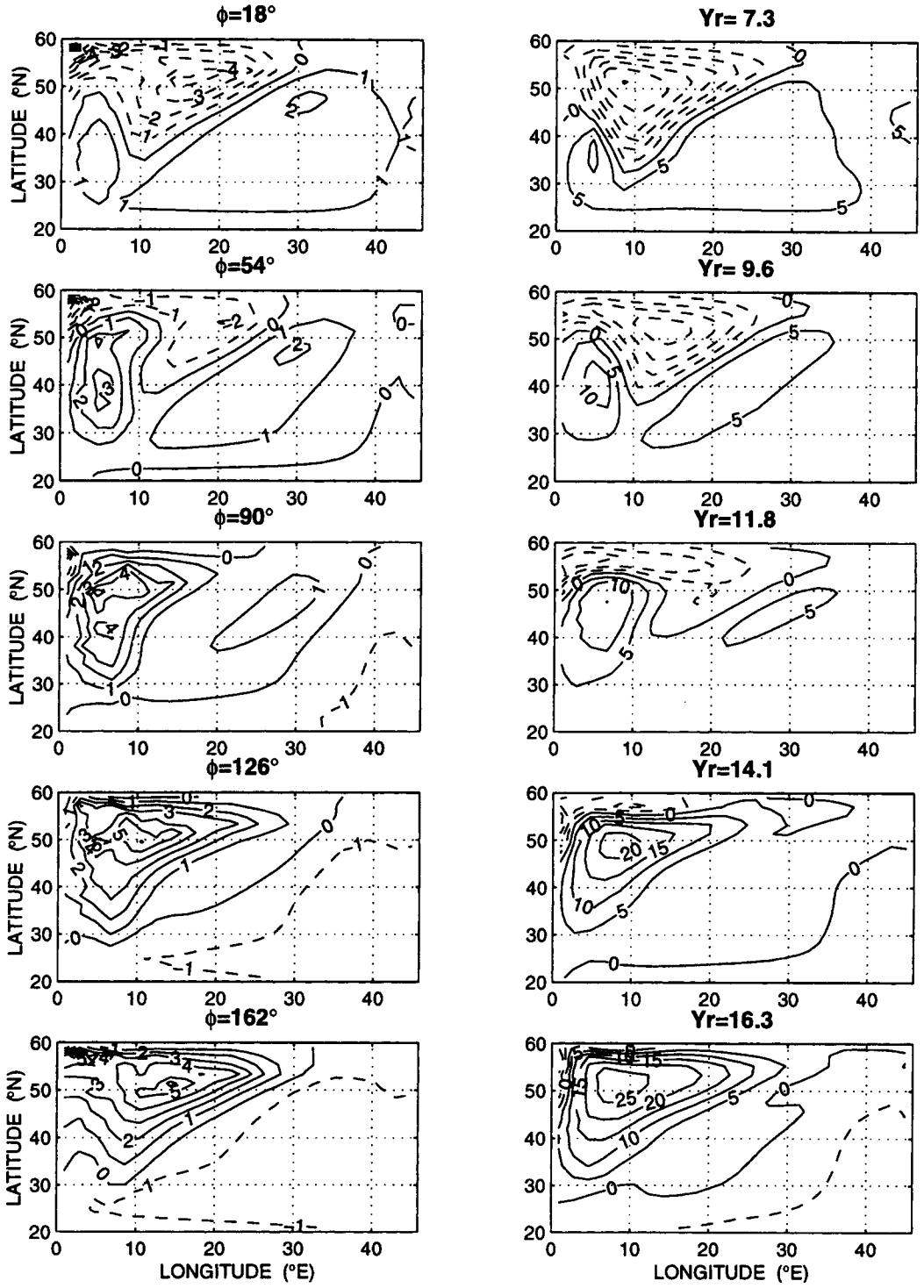

Fig. 5. Comparison of the time evolution of surface temperature ($z = -25$ m) during half a period for (*left column*) the unstable eigenmode $V(t) = \cos(\phi)V_r + \sin(\phi)V_i$ (the period is 25.3 years, while the growing time scale is 47.4 years) and (*right column*) the fully-developed oscillations under fixed surface heat flux diagnosed from the restoring experiment (the period is 22.5 years and its amplitude is stable after several hundreds of years). The phase has been been synchronized by looking at the projection of the model temperature anomalies on the real and imaginary part of the eigenmode: Model years correspond to Fig. 6.

is also very similar, maybe somewhat broader in meridional extension (50–60°N). This suggests that the change of surface boundary condition primarily affects the growth rate of basin modes that are already present but damped in the restoring case. This is clearly illustrated by the vertical profiles of the eigenmodes (Fig. 4): while the modes under fixed surface heat flux are all intensified at the surface, the modes under restoring boundary conditions see their amplitude strongly reduced in the upper hundred meters. Such a fundamental damping role of restoring boundary conditions on large scale ocean modes stresses the importance of a good parameterization of air-sea interactions for oceanic variability studies on interannual and longer time scales.

3.3. *Comparison of the unstable eigenmode and the model oscillation*

A detailed description of the nonlinear oscillations is provided in Greatbatch and Zhang (1995), Huck et al. (1999), Colin de Verdière and Huck (1999) and Huck et al. (2001), under both zonally-averaged surface heat flux and flux diagnosed at the end of a restoring run. The patterns and time evolution of the temperature anomalies differ slightly with the structure of the surface heat flux, as discussed in Huck et al. (1999): Mainly, westward-intensified diagnosed flux trap the surface anomalies in the north-west quarter, whereas zonally-uniform flux produce anomalies of larger zonal extent (eastward). At depth, the westward-propagating wave-like structure is very similar under both forcing, except for the southward extension along the western boundary under zonally uniform flux. Although only surface temperature anomalies are usually shown in the forward model integrations under diagnosed heat flux, indeed they compare very well with the time evolution of the linear unstable mode, at least visually. In addition, the deep temperature patterns and their propagation are found here to be also very similar (not shown).

In order to further compare the nonlinear oscillation under constant flux to the unstable eigenmode, we need to tune its phase and amplitude, which is not determined through our simple linear stability analysis. We compute the normalized projection coefficient of the model three-dimensional temperature anomalies field $T'(t)$ to the real and imaginary parts of the unstable eigenmode (V_r, V_i) as a function of time during the steady-amplitude oscillations:

$$C_r(t) = \frac{\langle T'(t), V_r \rangle}{(\langle \overline{T'(t'), T'(t')}^{t'} \langle V_r, V_r \rangle)^{1/2}}, \tag{8}$$

$$C_i(t) = \frac{\langle T'(t), V_i \rangle}{(\langle \overline{T'(t'), T'(t')}^{t'} \langle V_i, V_i \rangle)^{1/2}}. \tag{9}$$

The time evolution of these coefficients (Fig. 6) shows a good correlation of the anomaly field with the eigenmode in some phases of the oscillation (the correlation coefficient reach 90%). The phase relationship agrees well with the expected time evolution of the unstable eigenmode ($V_r \rightarrow V_i \rightarrow -V_r \rightarrow -V_i \rightarrow V_r \ldots$), although the time series are not as sinusoidal as the eigenanalysis theory assumes. This analysis also provides an estimate of the amplitude of the eigenmode in the fully-developed oscillations, since its scale is arbitrary in the linear stability analysis.

These time series allow us to "lock" the phases of the oscillations with the real and imaginary parts of the eigenmode, and to compare them. A reconstitution of various phases of the unstable eigenmode resembles the time evolution of temperature anomalies in the model oscillation remarkably well, as seen at the sea surface (Fig. 5), in the surface intensified vertical structure, and in the zonally-averaged latitude-depth plane (not shown). This implies that the structure of the fully developed model oscillation is indeed that of a linearly unstable eigenmode. It also suggests that the evolution of the nonlinear system may be determined by a form of Landau equation (Vallis, 1996) in which the oscillation frequency is determined essentially by linear dynamics and the amplitude of the equilibration is determined after a Hopf bifurcation by nonlinear terms. Nevertheless, the systematic derivation of any such lower order system is well beyond the scope of this paper.

3.4. *Other eigenmodes*

In the constant heat flux case, the second pair of conjugate eigenvalues (#4), damped on a 25.2 years time scale, has an oscillatory period of 14.6 years. The vertical structure of this mode is very similar to that of the unstable eigenmode (Fig. 3). The horizontal structure is also quite similar to that of the unstable mode except for the structure along the northern boundary, which is about

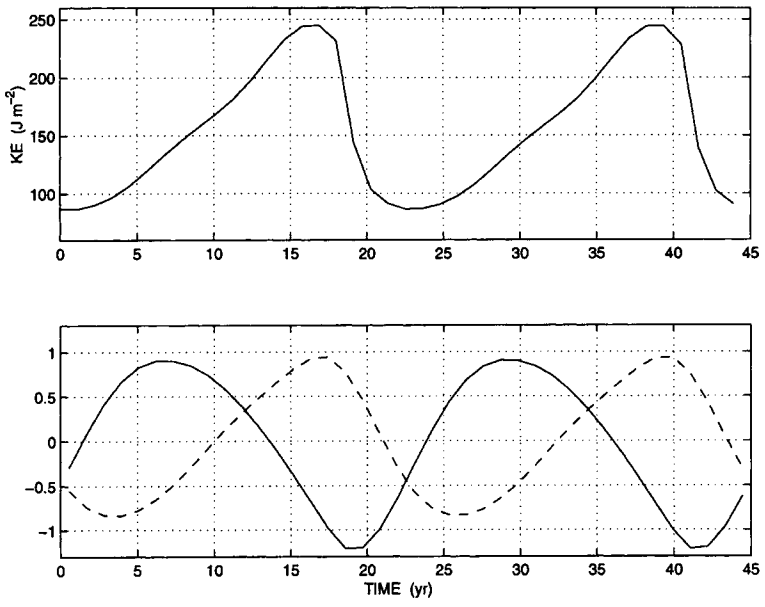

Fig. 6. (top) Evolution of kinetic energy as a function of time during two fully-developed oscillations of the model under fixed heat flux diagnosed at the end of the restoring run. (bottom) Normalized projection of the anomalous temperature field on the real (solid) and imaginary (dashed) part of the unstable eigenmode as a function of time (see text for details).

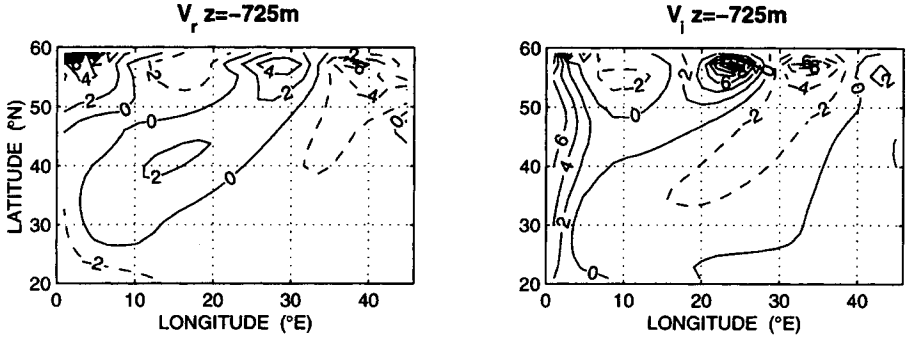

Fig. 7. Same as Fig. 4 for the most weakly damped oscillatory eigenmode (#4) at depth 725 m, whose period is 14.6 years and damping time scale 25.2 years. Notice the wavenumber 2 structure in longitude in contrast with a wavenumber 1 for the unstable eigenmode (#1).

wavenumber 2 in longitude and most noticeable around 700 m deep (Fig. 7). We expect indeed the damping to be enhanced through the higher horizontal dissipation on such smaller scales. However, in simulations at higher resolution and/or with reduced horizontal mixing, it is likely that these modes become unstable and generate other peaks in the variability spectrum, as is observed for instance in the next section experiments for the lowest diffusivity (Fig. 6). Thus, when more and more modes are allowed there is ready pathway to multiple time-scale variability.

4. Analysis around a bifurcation point

Rather than change the form of the surface boundary condition to produce an instability, we

now investigate the role of horizontal temperature diffusion when surface heat flux is prescribed as a linear function of latitude only (varying from 45 W m^{-2} at 20°N to −45 W m^{-2} at 60°N). Increasing the horizontal diffusivity damps the variability and allows a steady state to be constructed, but at the same time seems to have less influence on the structure and amplitude of the mean overturning circulation than the vertical diffusivity for instance. Thus, it is an appropriate parameter with which to examine some of the bifurcation properties of the system. As the diffusivity decreases, the real part of the most unstable eigenvalue increases and becomes finally positive. As the eigenvalue crosses the imaginary axis, the system evidently undergoes a supercritical Hopf bifurcation (Guckenheimer and Holmes, 1983) and the steady solution bifurcates into an unstable steady state and a stable limit cycle. A numerical continuation method would be necessary to follow further the stability of the limit cycle since the forward model integration does not allow to track unstable steady states, but this is beyond the scope of this paper.

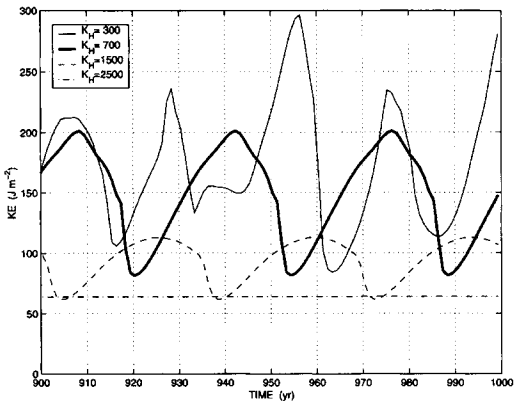

Fig. 8. Influence of the horizontal tracer diffusion K_H on the oscillations. The model is forced by constant surface heat flux, zonally uniform and varying linearly with latitude from 45 W m^{-2} at 20°N to −45 W m^{-2} at 60°N. For values of K_H lower than 500 m^2 s^{-1}, the oscillations are aperiodic with several spectral peaks, then they become periodic and monochromatic up to K_H = 2200 m^2 s^{-1}, while for larger diffusivity, the model ends up in a stable steady state.

4.1. *A crude bifurcation diagram*

We first run the model forward in time for coefficients of horizontal tracer diffusivity ranging from 300 to 3000 m^2 s^{-1} (Fig. 8). For values smaller than 2200 m^2 s^{-1}, perpetual oscillations are sustained while for larger values, the model settles down to a steady state after damped oscillations of comparable period. Huck et al. (1999) and Colin de Verdière and Huck (1999) conjectured that when the damping rate of temperature anomalies through diffusion reaches the growth rate of longwave baroclinic instability in the most unstable regions (western boundary current and eastward jet along the northern boundary) the planetary waves would no longer be unstable and the circulation tends to a steady state. Although the mean energy of the circulation does vary significantly with diffusion, the oscillation period is rather insensitive to it (Fig. 9).

The primary effect of horizontal diffusion on the mean state is to smooth out the temperature gradients and hence make the ocean circulation less energetic. Additionally, increasing diffusivity leads, by way of the warming of surface waters in the deep convection regions, to slightly warmer deep water masses. At the same time the warm pool cools, both through horizontal diffusion and because the fixed heat flux applied at the surface constrain the total basin heat-content to remain constant. Consequently the mean basin stratification is reduced, but the meridional overturning slightly increases because of the increased diapycnal component of the horizontal diffusion.

4.2. *Linear stability analysis*

For the model integrations with subcritical (i.e., larger) values of horizontal diffusivity that lead to a stable steady state, we perform a linear stability analysis that provides us with the least damped mode eigenvalue as a function of diffusion: As K_H decreases, the (negative) real part of the eigenvalue increases towards zero while the imaginary part barely changes (Table 2) as well as the spatial structure. This is typical of a supercritical Hopf bifurcation where a single eigenvalue crosses the real axis (in the complex plane) away from the origin.

Positive real parts of the eigenvalue are not obtained, since a numerical continuation method is necessary to follow the steady state as it becomes unstable for smaller (supercritical) values of the

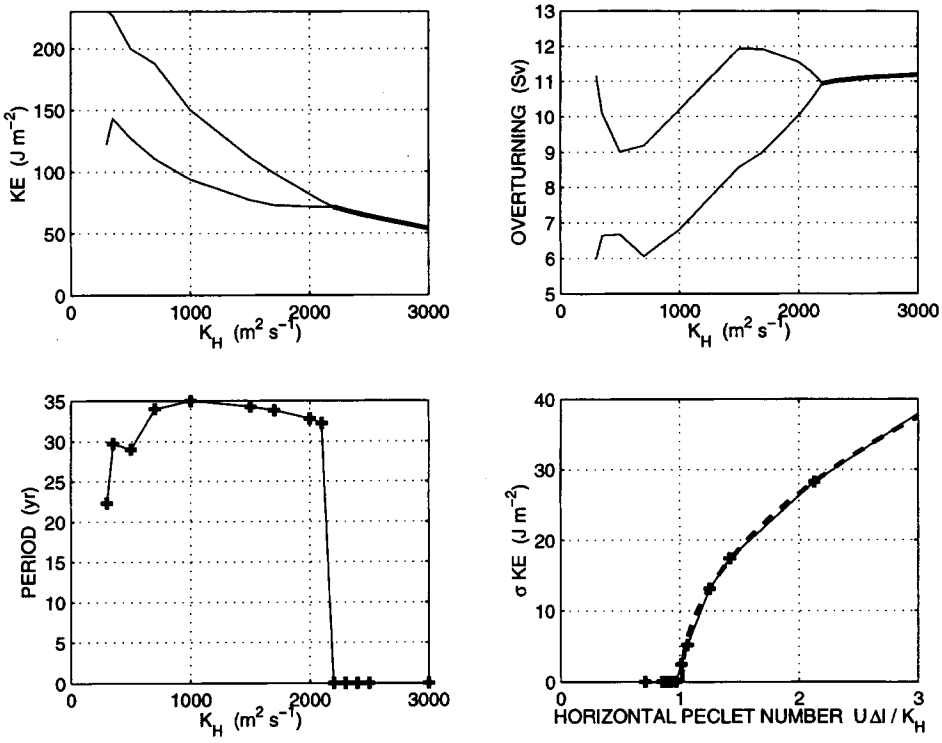

Fig. 9. Bifurcation diagram for the model forced by constant zonally uniform surface heat flux as a function of the horizontal tracer diffusion K_H: Solid thick lines are stable steady states, while thin lines are the extrema during oscillations of (a) total kinetic energy and (b) meridional overturning. (c) Period and (d) amplitude of the oscillations in terms of total kinetic energy standard deviation: a parabola (thick dashed line) has been fitted to the model points (thick cross) as a function of the horizontal Peclet number. Note that the oscillation period varies only slightly around the first bifurcation point at $K_H = 2200\ \mathrm{m^2\ s^{-1}}$. It is very likely that a secondary bifurcation occurs around $K_H = 500\ \mathrm{m^2\ s^{-1}}$ where the oscillations loose their regularity.

Table 2. *Most unstable eigenvalues (yr^{-1}) for different values of the horizontal tracer diffusivity K_H for the tangent linear matrix of the model under constant flux boundary conditions linearly varying with latitude*

K_H (m^2 s^{-1})	2200	2300	2400	2500
1	$1.61 \cdot 10^{-7}$	$7.25 \cdot 10^{-7}$	$6.63 \cdot 10^{-7}$	$5.93 \cdot 10^{-7}$
2	$-0.0050 \mp 0.2100i$	$-0.0074 \mp 0.2095i$	$-0.0097 \mp 0.2096i$	$-0.0131 \mp 0.2084i$
3	-0.0205	-0.0207	-0.0212	-0.0216
4	-0.0567	-0.0582	-0.0596	-0.0622
5	$-0.0736 \mp 0.0298i$	$-0.0755 \mp 0.0294i$	$-0.0777 \mp 0.0290i$	$-0.0795 \mp 0.0288i$

Note that the first pair of complex conjugate eigenvalues (#2) sees its real part tend to zero as K_H decreases, while its imaginary part is rather stable. The other eigenvalues do not vary significantly with K_H either. The first real eigenvalue $O(10^{-7})$ is associated with the conservation of the total heat content under constant flux boundary conditions.

diffusivity. This would in turn require differentiable equations of motion; the investigation of the use and influence of fully differentiable convection schemes (Schmidt and Mysak, 1996; Vellinga, 1996) would be a useful task for future work.

5. Analysis of the instability and the stabilizing processes

We now compare the period and growth rate of the unstable eigenmode with that of longwave baroclinic instability, and also assess the effects of surface restoring boundary conditions and horizontal tracer diffusion.

The oscillations have a rather complex spatial structure, with both global scale features and more localized extrema often located close to lateral boundaries. The evolution in the upper layers is clearly dominated by the response of the temperature field to changes in the intensity of the gyre, advecting warm waters from the south west corner along the western boundary and then eastward along the northern boundary. In contrast, the planetary wave structure is most likely seen at mid depth, away from energetic surface advection (see the 725 m section of the unstable eigenmode in Fig. 7). The westward propagation of such waves is not universal, and depends on the model forcing and parameters: the surface heat flux diagnosed from restoring boundary conditions are larger in the western regions and seem to trap the variability there, whereas using zonally uniform flux allow propagation of temperature anomalies all along the northern boundary (Greatbatch and Zhang, 1995; Huck et al., 2001). Baroclinic instability then amplifies the waves traveling westward in the northern region of the domain, sustaining the oscillations against dissipation. Given the 3-dimensional global structure of the linear unstable mode and the nonlinear oscillations, an interpretation in terms of baroclinic instability is more difficult to justify. Still, the vertical phase shift of the temperature anomalies and their phase lag with velocity anomalies, the source of temperature variance in the northwest quarter where the vertical shear is maximum, energy budgets, and the instability growth rate are all consistent with a form of baroclinic instability. Recently L. te Raa, H. Dijkstra and M. Schmeits (personal communication) have reexamined this instability of the thermally-driven circulation using techniques of numerical bifurcation theory. Their results closely agree with our interpretation, and a detailed analysis of the various terms in the equation for potential energy leads them to term the process a "generalized baroclinic instability," in part because of the importance of the basic state upwelling.

We have performed several other experiments with various parameters and forcing to test the agreement between the nonlinear model oscillations and unstable eigenmode of the tangent linear model. Wind forcing is introduced through zonal wind stress varying as an analytical function of latitude (Bryan, 1987). The results for standard and reduced vertical mixing ($K_V = 0.5 \times 10^{-4}\ m^2\ s^{-1}$), with and without wind forcing, show a relatively good agreement especially in terms of period (Fig. 10). However it seems that the weaker the growth rate, the larger the difference between the linear and nonlinear models growth rates: although more than 4 experiments would be required to confirm this trend, nonlinear processes are expected to be more influential for weaker instability. The oscillation periods we found in most of our experiments are in the range 17–33 years but depend on horizontal and vertical mixing coefficients and the presence or absence of wind forcing. However these might not be the most relevant for the real ocean because we considered only the influence of temperature on density. Using both temperature and salinity and a nonlinear equation of state of seawater, Greatbatch and Zhang (1995) reported oscillation periods of 50 to 70 years in an Atlantic-size ocean basin forced by realistic fluxes of heat, freshwater, and zonal wind stress.

In the standard experiment (Section 3), the unstable eigenmode has a growth time scale of 47.4 years, while the nonlinear model kinetic energy grows exponentially on a 58.4-years time scale for 200 years before the oscillations amplitude stabilizes. Evidently, the unstable eigenmode captures quite accurately the global instability growth rate. These growth rates are however much smaller than 'local" baroclinic instability calculations. That is to say, suppose we take the (zonal) shear and the stratification of one vertical column within the model, and suppose that this represents a steady solution in a zonally periodic domain. Using this as a basic state, we perform a conventional linear baroclinic instability analysis using

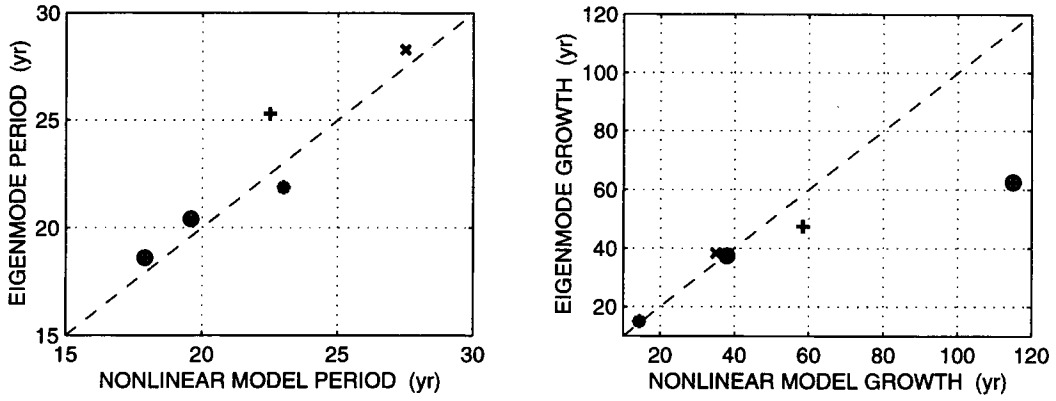

Fig. 10. Comparison of oscillations period and growth rate for the unstable eigenmode and the nonlinear model for different vertical diffusivities $K_V = 10^{-4}$ (+) and 0.5×10^{-4} (×) $m^2 s^{-1}$, with (○) and without wind forcing (zonal windstress according to Bryan, 1987). Also represented (*) is the result from a model of higher resolution (32 × 28 horizontally, 15 levels vertically) for $K_V = 10^{-4} m^2 s^{-1}$ and no wind forcing.

the quasigeostrophic equations. We find that the most unstable region is the latitude band 52°N–58°N, and this has a local growth rate reaching a few cycles per year, consistent with many previous studies of baroclinic instability. That is, local linear stability analyses typically show larger growth rates than the actual three-dimensional instability. The global instability cannot develop as fast as the most unstable local instability, apparently because of the global structure of the eigenmode.

We noted earlier that restoring surface boundary conditions damp both the oscillations in the nonlinear model and (consistently) the instability in the linear model. Now, the eigenvalues with "flux" and "restoring" conditions do not have a one-to-one correspondence, which makes direct comparison difficult. Further, it would be computationally prohibitively expensive to smoothly vary the surface conditions to go from one set of boundary conditions to the other. Thus, we somewhat heuristically assess the influence of changes in surface boundary conditions by looking at the changes in the eigenvalues and structure of the eigenmode whose physical structure in the restoring case is most similar to that of the unstable mode under fixed heat flux. In the unstable (fixed flux) case the mode is intensified at the surface and has an amplitude growing exponentially with height, the "same" mode, but now stabilized through surface relaxation, peaks around 300 m deep with an amplitude 3 times larger than at the surface. Instead of growing at a rate of 0.02 yr^{-1} in the fixed flux case, it is damped at 0.06 yr^{-1}, such that the restoring damping rate can be estimated as 0.08 yr^{-1}: This corresponds to a time scale of 12 years, equivalent to the time scale of the surface relaxation (35 W m^{-2} K^{-1}) applied to the whole depth of the basin. Similarly, the damping rate of the most unstable eigenmode under fixed heat flux (varying linearly with latitude) increases by 2.66×10^{-5} $yr^{-1}/(m^2 s^{-1})$ with horizontal tracer diffusivity close to the bifurcation point, such that a change of diffusivity by 1000 $m^2 s^{-1}$ corresponds to a damping time scale of 38 years, rather close to (and larger than) the actual growth rate of the unstable mode for $K_H = 700 m^2 s^{-1}$. Finally, we should mention that in reality there are additional potentially damping terms for the oscillations that are not considered here, like the bottom topography (Greatbatch et al., 1997), for which use of a primitive equation model will likely be necessary to explore.

6. Conclusions

We have demonstrated that the interdecadal oscillations of the thermally-driven ocean circulation in a flat-bottom ocean model forced by prescribed surface heat flux (as opposed to restoring boundary conditions) arise from a linearly unstable mode of the mean stratification and circulation. The oscillation in our nonlinear model

is typical of the oscillation found in a variety of models by various investigators when salinity is not considered.

The structure of the unstable eigenmode in the linear system is very similar to that found in the time-dependent, nonlinear, integration. Both are intense in the north-west part of the domain and in the upper hundreds of meters. The linear analysis predicts the three-dimensional structure of the mode, its time evolution and period, as well as its growth rate, but (of course) not its amplitude. The fully-developed oscillation period and structure is strikingly similar to that of the unstable mode, suggesting that nonlinearities are, at least in the numerical integrations, not influential in setting the structure or period, but only the amplitude of the oscillations.

Because of the difficulty in constructing an associated linear model, and the size of the associated eigenvalue problem, this type of analysis has rarely been performed in three-dimensional ocean models so far. Here, we have found it to be a useful tool for predicting model variability and large-scale instabilities, as well as an aid in understanding the underlying physical mechanisms. It seems possible that unstable or weakly damped eigenmodes of the large-scale ocean circulation could easily be excited by noise from either atmospheric synoptic systems or oceanic mesoscale eddies, and the structure and time scales of climate variability on decadal or interdecadal periods might be related to such eigenmodes. Nevertheless, these ideas are still very preliminary, and a full physical understanding of the structure and timescales of the unstable modes remains somewhat elusive. Certainly, a more complete as well as nonlinear analysis will be necessary to determine the processes that control the growth and the amplitude of the oscillations in the real ocean.

Notwithstanding all the caveats that we have mentioned throughout the paper (and the reader can certainly supply more) we are encouraged by the success of this method in predicting the period, structure and growth rate of large scale modes. As the construction of tangent linear models becomes more routine, and as computer power increases to enable such large eigenvalue calculations to be performed more routinely, it may become a useful member of the toolbox for oceanic and climatic stability and variability studies — just as linear calculations (and even normal mode calculations) can reveal much, but not all, about the structure of transient baroclinic eddies in the atmosphere and ocean. The main difficulty we foresee is that, if a higher resolution, perhaps even eddying model, could ever be used for such a study the instability analysis would reveal the presence of many smaller scale (e.g., baroclinic, barotropic) instabilities whose amplitude saturates and whose timescale is fast, which have little to do with the instability or structure of the thermohaline circulations. A challenge then will be to eliminate such "spurious" modes in a systematic fashion, leaving only the "interesting" thermohaline modes. Even if (or perhaps especially if) the thermohaline circulation of the ocean is stable under its present parameters, if it is a damped oscillator excited by either atmospheric or oceanic eddies then a linear analysis of a realistic simulation may tell us much about the potential for long-term oscillations and the variability of the atmosphere-ocean system.

7. Acknowledgments

This work has been supported by NSF ATM 9710285 grant. We wish to thank A. Colin de Verdière, T. Delworth, S. Garner and Jerôme Vialard, for their valuable comments and questions on a first draft of the manuscript. E. Tziperman and an anonymous reviewer are thankfully acknowledged for providing very useful suggestions to clarify the text and numerous references.

REFERENCES

Bryan, F. O. 1987. Parameter sensitivity of primitive equation ocean general circulation models. **17** 970–985.

Bryan, K. and Hansen, F. C. 1995. A stochastic model of North Atlantic climate variability on decade-to-century time scales. In: *Natural climate variability on decade-to-century time scales.* National Research Council, pp. 355–364.

Chen, F. and Ghil, M. 1996. Interdecadal variability in a hybrid coupled ocean–atmosphere model. *J. Phys. Oceanogr.* **26**, 1561–1578.

Colin de Verdière, A. and Huck, T. 1999. Baroclinic

instability: an oceanic wavemaker for interdecadal variability. *J. Phys. Oceanogr.* **29**, 893–910.

Colin de Verdière, A. and Huck, T. 2000. A 2 degree of freedom dynamical system for interdecadal oscillations of the ocean–atmosphere. *J. Cimate* **13**, 2801–2817.

Delworth, T., Manabe, S. and Stouffer, R. J. 1993. Interdecadal variations of the thermohaline circulation in a coupled ocean–atmosphere model. *J. Climate* 1993–2011.

Delworth, T. L. and Greatbatch, R. J. 2000. Multidecadal thermohaline circulation variability driven by atmospheric surface flux forcing. *J. Climate* **13**, 1481–1495.

Delworth, T. L. and Mann, M. E. 2000. Observed and simulated multidecadal variability in the North Atlantic. *Clim. Dyn.* **16**, 661–676.

Dijkstra, H. A., Molemaker, M. J., Van der Ploeg, A. and Botta, E. F. F. 1995. An efficient code to compute non-parallel steady flows and their linear stability. *Computers and Fluids* **24**, 415–434.

Dijkstra, H. A. and Molemaker, M. J. 1999. Imperfections of the North Atlantic wind-driven ocean circulation: Continental geometry and windstress shape. *J. Mar. Res.* **57**, 1–28.

Drbohlav, J. and Jin, F.-F. 1998. Interdecadal variability in a zonally averaged ocean model: an adjustment oscillator. *J. Phys. Oceanogr* **28**, 1252–1270.

Fanning, A. F. and Weaver, A. J. 1998. Thermohaline variability: the effects of horizontal resolution and diffusion. *J. Climate* **11**, 709–715.

Giering, R. 1999. *Tangent linear and adjoint model compiler.* TAMC 5.2 Users manual version 1.4, MIT Center for Global Change Science, 64 pp (http://puddle.mit.edu/ralf/tamc).

Greatbatch, R. J. and Zhang, S. 1995. An interdecadal oscillation in an idealized ocean basin forced by constant heat flux. *J. Climate* **8**, 81–91.

Greatbatch, R. J. and Peterson, K. A. 1996. Interdecadal variability and oceanic thermohaline adjustment. *J. Geophys. Res.* **101**, 20,467–20,482.

Greatbatch, R. J., Peterson, K. A. and Roth, H. 1997. *Interdecadal variability in a coarse resolution model with North Atlantic bottom topography.* Technical Report, Department of Oceanography, Dalhousie University, Halifax, Nova Scotia, Canada.

Guckenheimer, J. and Holmes, P. 1983. *Nonlinear oscillations, dynamical systems, and bifurcations of vector fields.* Applied Mathematical Sciences **42**, Springer-Verlag, New York, 459 pp.

Haney, R. 1971. Surface thermal boundary condition for ocean circulation models. *J. Phys. Oceanogr.* **1**, 241–248.

Huang, R. X. and Chou, R. L. 1994. Parameter sensitivity of the saline circulation. *Clin. Dyn.* **9**, 391–409.

Huck, T., Colin de Verdière, A. and Weaver, A. J. 1999. Interdecadal variability of the thermohaline circulation in box-ocean models forced by fixed surface fluxes. *J. Phys. Oceanogr.* **29**, 865–892.

Huck, T., Vallis, G. K. and Colin de Verdière, A. 2001. On the robustness of the interdecadal modes of the thermohaline circulation. *J. Climate* **14**, 940–963.

Kerr, R. A. 2000. A North Atlantic climate pacemaker for the centuries. *Science* **288**, 1984–1986.

Klinger, B. A., Marshall, J. and Send, U. 1996. Representation of convective plumes by vertical adjustment. *J. Geophys. Res.* **101**, 18,175–18,182.

Kushnir, Y. 1994. Interdecadal variations in North Atlantic Sea Surface Temperature and associated atmospheric conditions. *J. Climate* **7**, 141–157.

Malkus, W. R. 1972. *Non-periodic convection at high and low Prandtl number.* Mémoires Société Royale des Sciences de Liège, 6° série, IV, pp. 125–128.

Mann, M. E., Bradley, R. S. and Hughes, M. K. 1998. Global-scale temperature patterns and climate forcing over the past 6 centuries. *Nature* **392**, 779–787.

Meacham, S. P. 2000. Low-frequency variability in the wind-driven circulation. *J. Phys. Oceanogr.* **30**, 269–293.

Mikolajewicz, U. and Maier-Reimer, E. 1990. Internal secular variability in an ocean general circulation model. *Clin, Dyn.* **4**, 145–156.

Miller, R. N., Zaron, E. D. and Bennett, A. F. 1994. Data assimilation in models with convective adjustment. *Mon. Wea. Rev.* **122**, 2607–2613.

Quon, C. and Ghil, M. 1992. Multiple equilibria in thermosolutal convection due to salt-flux boundary conditions. *J. Fluid Mech.* **245**, 449–483.

Samelson, R. M. and Vallis, G. K. 1997a. Large-scale circulation with small diapycnal diffusion: the two-thermocline limit. *J. Mar. Res.* **55**, 223–275.

Samelson, R. M. and Vallis, G. K. 1997b. A simple friction and diffusion scheme for planetary geostrophic basin models. *J. Phys. Oceanogr.* **27**, 186–194.

Schmidt, G. A. and Mysak, L. A. 1996. The stability of a zonally averaged thermohaline circulation model. *Tellus* **48**, 158–178.

Seager, R., Kushnir, Y. and Cane, M. A. 1995. On heat flux boundary condition for ocean models. *J. Phys. Oceanogr.* **25**, 3219–3230.

Sheremet, V. A., Ierley, G. R. and Kamenkovich, V. M. 1997. Eigenanalysis of the two-dimensional wind-driven ocean circulation problem. *J. Mar. Res.* **55**, 57–92.

Stammer, D. and Wunsch, C. 1996. The determination of the large-scale circulation of the Pacific Ocean from satellite altimetry using model Green's functions. *J. Geophys. Res.* **101**, 18,409–18,432.

Timmermann, A., Latif, M., Voss, R. and Grötzner, A. 1998. Northern hemispheric interdecadal variability: a coupled air–sea mode. *J. Climate* **11**, 1906–1931.

Tziperman, E., Thacker, W. C., Long, R. B. and Hwang, S.-M. 1992. Oceanic data analysis using a general circulation model. Part I: Simulations. *J. Phys. Oceanogr.* **22**, 1434–1457.

Tziperman, E., Toggweiler, J. R., Feliks, Y. and Bryan, K. 1994. Instability of the thermohaline circulation with respect to mixed boundary conditions: Is it really a

problem for realistic models? *J. Phys. Oceanogr.* **24**, 217–232.

Tziperman, E., 1997. Inherently unstable climate behaviour due to weak thermohaline ocean circulation. *Nature* **386**, 592–595.

Vallis, G. K. 1996. From laminar flow to turbulence. In: *An introduction to nonlinear physics* (ed. L. Lam). Springer-Verlag, pp. 308–357.

Vellinga, M. 1996. Instability of two-dimensional thermohaline circulation. *J. Phys. Oceanogr.* **26**, 305–319.

Weaver, A. J. and Sarachik, E. S. 1991. Evidence for decadal variability in an ocean general circulation model: an advective mechanism. *Atmos. Oceans* **29**, 197–231.

Weaver, A. J., Sarachik, E. S. and Marotzke, J. 1991. Freshwater flux forcing of decadal and interdecadal oceanic variability. *Nature* **353**, 836–838.

Winton, M. 1996. The role of horizontal boundaries in parameter sensitivity and decadal-scale variability of coarse-resolution ocean general circulation models. *J. Phys. Oceanogr.* **26**, 289–304.

Wright, D. G. and Stocker, T. F. 1991. A zonally averaged ocean model for the thermohaline circulation. Part I: model development and flow dynamics. *J. Phys. Oceanogr.* **21**, 1713–1724.

Wright, D. and Stocker, T. 1992. Sensitivities of a zonally-averaged global ocean circulation model. *J. Geophys. Res.* **97**, 12,707–12,730.

Zou, X. 1997. Tangent linear and adjoint of "on–off" processes and their feasibility for use in 4-dimensional variational data assimilation. *Tellus* **49A**, 3–31.